Localized Radon Transform-Based Detection of Ship Wakes in SAR Images

Anthony C. Copeland, Gopalan Ravichandran, and Mohan M. Trivedi, *Senior Member, IEEE*

Abstract— **This paper presents a Radon transform-based approach to the detection of ship wakes in Synthetic Aperture Radar (SAR) images. The key element of this technique is a localization of the Radon transform, whereby the intensity integration is performed over short line segments rather than across the entire image. A linear feature detection algorithm, which utilizes this localized Radon transform, is then developed. In this algorithm, referred to as the feature space line detector (FSLD) algorithm, the transform space is subjected to processing which server to isolate and locate the response of linear features and suppress the responses of false alarms. This algorithm is tested on both synthetic images corrupted by various levels of Weibull multiplicative noise and on actual SAR images of ship wakes. The results of this testing demonstrate the algorithm's robustness in the presence of noise, as well as its ability to detect and localize linear features that are significantly shorter than the image dimensions.**

I. Introduction

THIS paper describes the development of an algorithm to automatically detect ship wakes in digital Synthetic Aperture Radar (SAR) images of the ocean surface. Although the ship itself can often be seen as a bright region close to the wake pattern, there are at least two reasons why it would be more advantageous to detect the wake pattern rather than the ship itself [1]: the wake pattern is larger and more distinct than the ship signature, and it can yield a better estimate of the ship's true location. The latter is true because the motion of the ship in the ocean causes it to appear in the SAR image displaced in azimuth from its actual location, since conventional SAR image reconstruction techniques assume no motion of objects in the image scene. The ship wake pattern can also yield information about the ship's heading and speed.

Although a ship moving through a body of water normally creates a characteristics V-shaped pattern of waves, the actual appearance of a ship wake pattern in a SAR image is extremely variable. The wake pattern can be divided into several components, some of which may or may not always be visible in a SAR image [1]. The principal components are the Kelvin wake, which is itself composed of the cusp waves, divergent waves, and transverse waves; the turbulent wake, which comprises the turbulent region directly behind the ship; and the narrow-V wake, which occurs when ambient gravity waves are reflected off the turbulent wake and augment the incoming ambient waves. In water where the conditions are right, there may also be ship-generated internal wave wakes. These are subsurface waves located at the boundary between two layers of water of differing density or temperature. These internal waves cause small ripples on the surface which may make them detectable in a SAR image [2]. Not all of these wake components are visible in every image, due to different orientations to the SAR sensor, variations in ship size and speed, as well as varying ocean and wind conditions. This means that the actual wake pattern present can vary greatly, complicating the problem of automatic detection. However, wake components usually appear as linear features in SAR imagery. Thus, our approach was to locate ship wakes by identifying these linear features.

The problem now is one of linear feature detection. These linear features not only have a certain finite length but also a breadth. Such a linear feature can be defined as a long, narrow region of pixels that are, in general, of a different intensity than the background. This linear feature can be either brighter or darker than the background, and does not necessarily have to be straight. This description was considered in the development of the linear feature detector. Another important consideration was the high level of inherent multiplicative noise, or speckle, that characterizes SAR imagery. Since this noise can only be reduced at the expense of image resolution [3], it is beneficial to use a feature detection algorithm that is robust in the presence of this noise.

The detection of linear features is often treated as if it were an edge detection problem, i.e., linear features are found by looking for their edges [4]. The edge-based approach is to apply an edge operator to the image, then to perform edge linking to group the disconnected edge elements into structure boundaries that can be interpreted [5]. There are several different edge operators that are commonly used, but in each case, the edge operator has a small spatial extent and is designed to detect the presence of a local edge in the image. This type of local operation is rendered less effective for an image with a high level of noise variance (power). Every sharp intensity change in the noise will indicate a local edge. Operations that depend on more global information should be less affected by such local noise variations. Additionally, the edge linking process is a complex problem that must be governed by some set of rules, or constraints. These constraints are what define a particular edge linking technique. Regardless of which technique is chosen the edge linking process is a difficult, error prone, and computationally expensive task [6].

Manuscript received March 3, 1994.

The authors are with the Computer Vision and Robotics Research Laboratory, Electrical and Computer Engineering Department, University of Tennessee, Knoxville, TN 37996-2100 USA.

IEEE Log Number 9406432.

The approach in this paper avoids edge detection and linking by detecting the linear features directly. The image is first subjected to a localized Radon transform, which maps the image into a feature space, or transform domain. Then this transform domain is subjected to processing and analysis to locate the responses caused by the presence of linear features in the original image. This scheme for linear feature detection was presented in a previous paper [7]. As applied to SAR imagery, this approach is most suited for a steep-depression system, where feature edge information is less likely to be obscured by shadow effects.

A great deal of research has been dedicated to developing Radon transform-based algorithms for linear feature detection, and specifically for ship wake detection in SAR images. Reference [3] computed the Radon transform of SAR images of ship wakes and ocean waves, applied an enhancement operator within the transform space, and then used the filtered-backprojection algorithm to compute the inverse Radon transform. The result was that the linear features in the images appeared far more prominent against the background and the speckle noise was significantly reduced. The enhancement operator simply squared the difference between each value in the transform domain and the mean. Reference [8] presented a procedure utilizing a 13×13 window and an adaptive threshold for the detection of peaks and troughs within the transform space. They also calculate the probability of detecting a line with their method based on the relative length and intensity of the line. They have applied their method to both synthetic test images and to a SAR image of a forest.

References [9], [10] presented methods for detection of ships and ship wakes in SAR images of coastal regions. First, digital maps are used to distinguish sea from land in the images. Then actual ship signatures are detected by an adaptive filter that steps a frame across the image looking for pixels of an intensity greater than a certain threshold. Starting at the locations of these detected ships, a search for their associated wakes is performed by calculating the intensity mean along lines extending out in every direction. Finally, false alarms are rejected using an homogeneity test. Reference [11], used the Hough transform to detect ship-generated internal waves in SAR images. First, the SAR images were filtered by a 2-D highpass filter. Then the Hough transform was performed and the resulting transform space was thresholded to obtain the brightest 100 points. A clustering algorithm was then applied to group together points resulting from the same internal wave feature.

Reference [1], used the Radon transform augmented with preprocessing and postprocessing to detect ship wakes in Seasat SAR images. The preprocessing consisted of a running mean filter applied to the input image which served to remove the effects of low-frequency components. The authors claim that this filter served to double the signal-to-noise ratio (SNR) of the input image. The postprocessing consisted of a peak detector based on the Wiener filter applied to the transform data. In a follow-on paper [12], the Dempster–Shafer method of data fusion was applied to the output from the Wiener filter to classify the detected linear features as to whether or not they belong to a ship wake. More recently, [13] applied both one-dimensional and two-dimensional adaptive correlation enhanced (1DACE and 2DACE) algorithms to SAR images to reduce noise and improve the visibility of ship wakes. Then a ship wake detection algorithm was applied to the filtered images. The Radon transform was applied to the images, the data was thresholded, and each distinct region was isolated and assigned to a class. The angle coordinates of the individual classes are then examined to determine whether the class likely represents a ship wake.

Most of this recent work on SAR ship wake detection focused on prefiltering the SAR data in an attempt to make wake features more distinct, and then applying a linear feature detection algorithm. In addition, the detection of linear wake features that display a considerable amount of curvature or that do not span a significant portion of the SAR images has not been considered. The work described in this paper attempts to avoid prefiltering the images with a detection scheme that is robust in the presence of typical SAR noise. Also, this detection scheme is intended specifically to identify wake features which are short, curved, or that lie only partially in the SAR image.

Section II of this paper provides some basic technical background of the Radon transform, and details the motivation for the development of a localization of this transform to better accentuate linear features of lengths significantly less than the image dimensions. Section III discusses in more detail the approach taken toward linear feature detection and describes the algorithm developed to accomplish this. Section IV presents experimental results of testing this algorithm on both synthetic test images and actual SAR images of ship wakes. Section V concludes the paper, and suggests future research directions.

II. Localizing the Radon Transform

The Radon transform on Euclidean space was first established in [14]. This work was concerned with determining the internal distribution of some characteristic of a 2-D or 3-D object from a set of projected distributions, or profiles, of that characteristic oriented at various angles. Nearly a half century after Radon's work, the Hough transform for detecting straight lines in digital pictures was introduced [15]. Reference [16] observed that the Hough transform is actually just a special case of the Radon transform. It is true, however, that many researchers in this area who make use of this technique still refer to it as the Hough transform.

A. Definition of the Radon Transform

The Radon transform over a two-dimensional Euclidean space can be defined as [1]:

$$\check{f}(\theta, \rho) = \Re\{f\} = \int \int_D f(x, y)\delta(\rho - x\cos\theta - y\sin\theta)dydx \tag{1}$$

where

- D is the entire x–y image plane,
- $f(x, y)$ is the image intensity (gray level) at position (x, y),

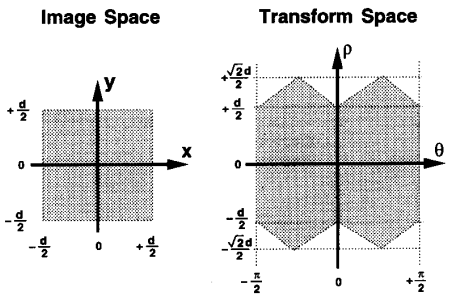

Fig. 1. The transform space resulting from the Radon transform of a $d \times d$ image.

- δ is the Dirac delta function,
- ρ is the length of the normal from the origin to the straight line,
- θ is the angle between the normal and the x-axis.

The Radon transform accentuates linear features in an image by integrating image intensity along all possible lines in an image. The presence of the Dirac delta function forces the integration of $f(x, y)$ along a line whose normal representation is $\rho = x \cos\theta + y \sin\theta$. In the normal representation of a line, ρ is the length of the normal from the origin to the line and θ is the angle the normal forms with respect to the x-axis.

Fig. 1 shows the transform space that results from the Radon transform of a square $d \times d$ image. This is the convention that will be used for displaying Radon transforms throughout this paper. The origin is considered to be the center of the image space. The transform is defined for all values of ρ and θ that represent lines lying at least partially on the image space D. To represent every possible straight line in the image, it is necessary to vary θ from $-\frac{\pi}{2}$ to $+\frac{\pi}{2}$ and to vary ρ from $-\frac{\sqrt{2}d}{2}$ to $+\frac{\sqrt{2}d}{2}$. In this paper, however, the ρ parameter varies only from $-\frac{d}{2}$ to $+\frac{d}{2}$ creating a nice rectangular transform space that is easier to analyze. This means only that linear features lying just partially in the far corners of an image are not represented.

B. Properties of the Radon Transform

It may be useful to consider some simple properties of this parameter transform noted in [16] that follow directly from the definition:

1) If $f(x, y)$ is concentrated at a point (x_0, y_0) then $\check{f}(\theta, \rho)$ is nonzero along a sinusoidal curve $\rho = x_0 \cos\theta + y_0 \sin\theta$.
2) A given point (θ_0, ρ_0) in the transform domain corresponds to a line in the x–y plane defined by $\rho_0 = x \cos\theta_0 + y \sin\theta_0$.
3) Collinear points in the x–y plane along the line parameterized by θ_0 and ρ_0 map to sinusoidal curves in the θ-ρ plane, and these curves all intersect at the point (θ_0, ρ_0).
4) Points lying along the curve $\rho = x_0 \cos\theta + y_0 \sin\theta$ in the θ-ρ plane correspond to lines in the x–y plane that all pass through the point (x_0, y_0).

The Radon transform should therefore contain a peak corresponding to every line in the image that is brighter than its surroundings, and a trough for every dark line. Thus, the problem of detecting lines is reduced to detecting these peaks and troughs in the transform domain. The Radon transform is particularly suited for finding lines in images characterized by a large amount noise. It tends to cancel our intensity fluctuations due to noise by the integration process [3]. A consequence of this is that one may expect the signal-to-noise ratio of the Radon transform space to be greater than that of the image itself [1].

C. Drawbacks of the Radon Transform

There are some drawbacks to using the Radon transform for linear feature detection. Since the intensity integration is performed over the entire length of the image, it can have difficulty detecting line segments which are significantly shorter that the image dimensions [3]. It also has no capability of providing information about the positions of the endpoints of these shorter line segments, or on line length. And linear features that span across the entire image but display some curvature may not produce suitable peaks or troughs in the transform domain. These problems are even more significant when the transform is applied to an image with a high level of noise.

These drawbacks can have an adverse effect on attempts to analyze SAR imagery containing ship wakes. Although ship wake components usually appear straight when viewed over a short distance, they can display significant curvature over time due to changes in ship headings, water depth, or ocean conditions. And if the image has been cropped to optimally display the ship wake of interest, performing an integration across the entire image is sufficient to produce suitable peaks and troughs in the transform space. But in an automated system to continuously analyze SAR data to search for ship wakes, the wakes would not always span the entire image so nicely.

To illustrate this deficiency of the Radon transform, consider Fig. 2. Each of the 128 × 128 synthetic test images contain two line segments that intersect at an angle of approximately 20° (similar to a ship wake). In Fig. 2(a) the line segments span the entire length of the image. In Fig. 2(b), the length of the line segments is about one-half the image dimensions ($\frac{d}{2} = 64$ pixels), and in Fig. 2(c) the length is $\frac{d}{4}$. Each of these test images was corrupted with the same random noise function, and then a Radon transform was performed on each. We can see that the Radon transform in Fig. 2(a) contains two relatively distinct peaks corresponding to the two lines the test image, despite the high level of noise present. But as the line length is decreased to $\frac{d}{2}$ and then to $\frac{d}{4}$, the peaks become far less distinct.

We wish to modify the Radon transform so as to localize the area in which each integration takes place. This will reduce the problem of integrating through more noise than is necessary, which tends to obscure the peak (or trough) corresponding to a linear feature that is much shorter than the image dimensions. It can also produce better results if the ship wake components display some curvature.

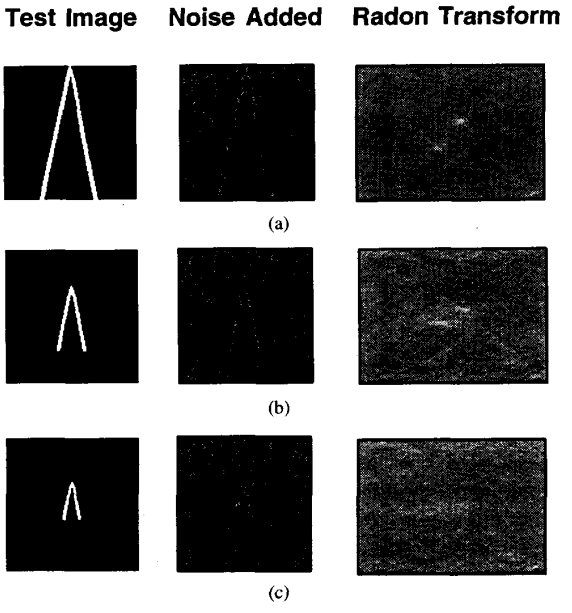

Fig. 2. Radon transforms of lines of various lengths in a noisy background. This demonstrates how lines that are much shorter than the image dimensions can be obscured in the transform domain by a high level of noise.

D. Definition of the Localized Radon Transform

One way to accomplish this localization is to perform the Radon transform in a small window, which can be shifted throughout the image. The window size should be small enough to detect lines of the desired length, and the windows should overlap to provide good coverage of the entire image space. This method requires the computation of a large number of individual Radon transforms. Such a "multiple window" parameter transform is described in [17]. A method that is conceptually similar but easier to implement is to compute the transform over the entire image in the space domain, but to place appropriate limits on the integration. The effect of these limits is that the intensity integration is performed over a line segment, instead of a line.

This localized Radon transform can be represented as the original transform (1) with limits on the integration, and with an additional parameter:

$$\check{f}(\theta,\rho,\sigma) = \Re_{\mathrm{Loc}}\{f\} = \int_{x_{\min}}^{x_{\max}} \int_{y_{\min}}^{y_{\max}} f(x,y)\delta(\rho - x\cos\theta - y\sin\theta)dydx \tag{2}$$

where

- $x_{\min} = \min(\rho\cos\theta - \sigma\sin\theta, \rho\sin\theta - (\sigma+\lambda)\sin\theta)$,
- $x_{\max} = \max(\rho\cos\theta - \sigma\sin\theta, \rho\sin\theta - (\sigma+\lambda)\sin\theta)$,
- $y_{\min} = \rho\sin\theta + \sigma\cos\theta$,
- $y_{\max} = \rho\sin\theta + (\sigma+\lambda)\cos\theta$,
- σ is a shift parameter,
- λ is the length of the line segment of integration (LSOI).

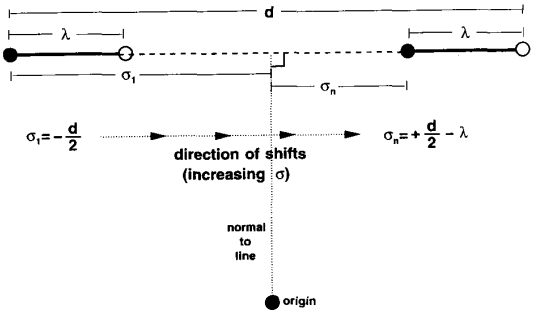

Fig. 3. Definition of the σ and λ parameters. σ represents the distance the LSOI is shifted along the line, and λ is simply the length of the LSOI.

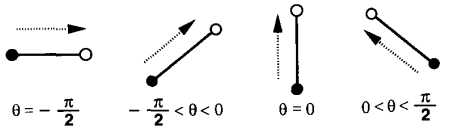

Fig. 4. Definition of the positive direction for the σ parameter. This direction depends on the orientation of the line.

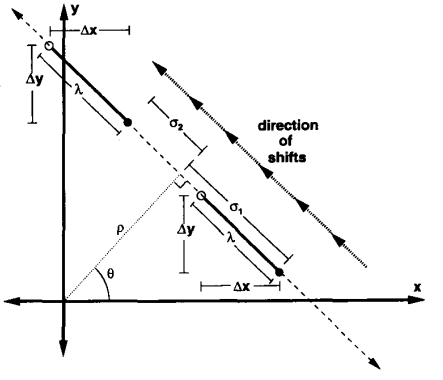

Fig. 5. Example of shifting the LSOI. In this case, the positive shift direction is up and to the left, corresponding to an increasing σ.

The additional parameter creates a transform space that is now three-dimensional. σ represents the point along the line represented by θ and ρ where the integration begins, or the distance the LSOI has been shifted along the line. λ is simply the length of the LSOI. Fig. 3 shows these parameters.

The magnitude of σ is the distance from the beginning point of the LSOI (the solid black point) to the point at which the line intersects its normal. In order to represent every line segment in the image, it is necessary to vary σ from $-\frac{\sqrt{2}d}{2}$ to $+\frac{\sqrt{2}d}{2} - \lambda$, but to simplify the transform space this parameter is shifted only within the interval $-\frac{d}{2}$ to $+\frac{d}{2} - \lambda$. As the LSOI is shifted in a positive direction, the σ parameter increases. The positive shift direction for the σ parameter is defined in Fig. 4. This direction depends on the orientation of the line. Fig. 5 shows an example of shifting the LSOI. In this case, $\sigma_1 < 0$ and $\sigma_2 > 0$. The $\Delta x = x_{\max} - x_{\min} = |\lambda\sin\theta|$ and $\Delta y = y_{\max} - y_{\min} = \lambda\cos\theta$ terms represent the extent of the integration.

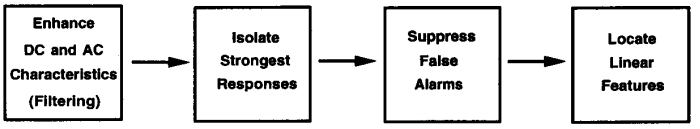

Fig. 6. The general approach toward linear feature detection that was chosen.

The $x_{\min}$ and $x_{\max}$ terms in (2) depend on the value of θ. When $-\frac{\pi}{2} < \theta < 0, x_{\min} = \rho\cos\theta - \sigma\sin\theta$ and $x_{\max} = \rho\cos\theta - (\sigma + \lambda)\sin\theta$. When $0 < \theta < +\frac{\pi}{2}$, these two values reverse. This is necessary to keep the upper integration limit for x higher than the lower integration limit. As long as θ is only sampled between $-\frac{\pi}{2}$ and $+\frac{\pi}{2}$, the $x_{\min}$ and $x_{\max}$ values never need to be switched (since $\cos\theta$ never drops below zero in this interval). It is important to note also that if the line is perfectly horizontal ($\theta = -\frac{\pi}{2}$) the $y_{\min}$ and $y_{\max}$ terms are equal, and if the line is perfectly vertical ($\theta = 0$) the $y_{\min}$ and $y_{\max}$ terms are equal, meaning that the value of the double integral is zero. In these two special instances, this value is assumed to be the summation of pixel intensities directly along that horizontal row or vertical column (since the image is actually a discrete space).

E. Computational Complexity

This localization of the Radon transform prevents us from using the popular frequency domain calculation method [3] to save computation time. However, the number of multiplications required is only slightly larger than for the normal "accumulator bin" method of calculating the Hough transform. In this method, each image point (x, y) is considered in turn, and the value of ρ is calculated for each value of θ to be considered. The accumulator bin in the transform domain corresponding to each $\theta - \rho$ pair is incremented by the gray-level intensity of pixel (x, y). Our method for calculating the localized Radon transform is similar, except that each pixel (x, y) is first checked to see if it lies within the current integration limits. The "shifting" of the LSOI is actually accomplished by incrementing the integration limits, requiring no additional multiplications.

III. The Feature Space Line Detector (FSLD) Algorithm

A. General Approach Toward Detection

As mentioned earlier, a true linear feature in an image not only has length but also breadth. It can have variable lengths and widths, but it is the sharpness of its edges that determines its distinctness in the image. In the frequency domain, we can think of a linear feature as an area in the image that has a distinctly high (or low) dc content in the longitudinal direction, and a relatively high ac content in the transverse direction. The dc energy represents the mean intensity of pixels, and the ac energy represents all nonzero frequencies which combine to create edges in the image.

TABLE I
Frequency Domain Definition of a Linear Feature

Frequency Content	Longitudinal Direction	Transverse Direction
DC	high or low	n/a
AC	n/a	high

Table I shows this frequency-domain definition of a linear feature. Note that we can't describe the ac content in the longitudinal direction, since the feature may or may not be continuous. We also can't describe the dc content in the transverse direction since this depends mostly on the mean pixel intensity of the background, which can be variable.

Fig. 6 shows the general approach toward detection that was chosen for this research. First, the characteristics which define a linear feature are enhanced. This creates a transform domain in which we can see where these particular characteristics are strongest. Then these areas of the transform domain are isolated as potential indications of linear features. An attempt is made to exclude false alarms by testing each area of strong responses and excluding those which don't meet certain criteria. Then the linear features corresponding to the remaining responses are mapped back into the original image domain in the proper locations.

B. Overview of Implementation

The algorithm presented here will be referred to as the Feature Space Line Detector (FSLD) algorithm, since the analysis to detect linear features takes place within the feature space, or Radon transform domain. The FSLD algorithm can be stated as follows:

For each value of θ:

1) Perform a localized Radon transform on image for one θ only.
2) Calculate the variance along strips in the ρ direction.
3) Threshold the transform domain.
4) Perform morphology on the transform domain.
5) Reconstruct lines in image domain.

Since each value of θ is considered individually, the processing is performed on only a 2-D segment of the three-dimensional transform domain. This transform domain processing can best be explained by examining what happens to one specific transform segment. Fig. 7 shows the results when the algorithm is performed on the 256 × 256 SAR image shown for the case where $\theta = -82°$. This value of

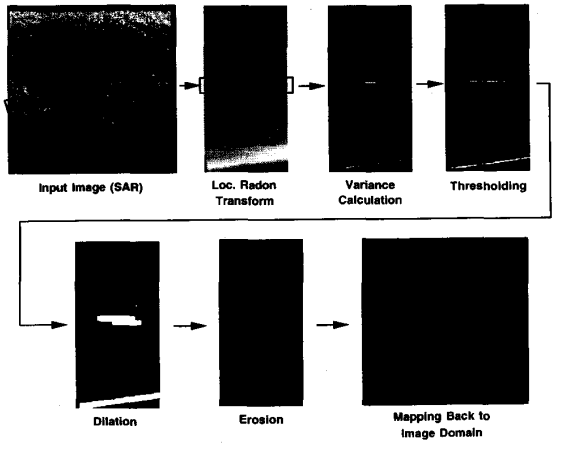

Fig. 7. The transform domain processing for the $\theta = -82°$ segment.

θ corresponds to the orientation of the ship wake component that is outlined. The integration length was $\lambda = \frac{d}{2} = 128$ pixels. In the 2-D segment of the transform domain, the ρ parameter varies vertically as before, and the σ parameter varies horizontally from $\sigma_{\min} = -\frac{d}{2}$ to $\sigma_{\max} = +\frac{d}{2} - \lambda$. Notice that since the wake component is a dark linear feature, it appears in the transform domain as a narrow dark region bordered above and below by brighter regions. The horizontal "streaking" results from varying the σ parameter and shifting the LSOI onto, across, and off of the wake component. The result is that the input image has been low-pass filtered, removing nearly all ac energy oriented at $\theta = -82°$.

The variance calculation is performed along short segments in the vertical (ρ) direction only. This process can be thought of as high-pass filtering or as an edge detection operation, accentuating areas in the transform domain containing sharp changes along the ρ direction. Equation (3) represents this variance calculation:

$$\check{f}_{\text{var}}(\theta, \rho, \sigma) = \int_{\rho-(v/2)}^{\rho+(v/2)} (f(\theta, \rho, \sigma) - \check{f}_{\text{mean}}(\theta, \rho, \sigma))^2 d\rho \tag{3}$$

where

- $\check{f}(\theta, \rho, \sigma)$ is the localized Radon transform of the input image $f(x, y)$,
- v is the distance over which the variance calculation is performed,
- and $\check{f}_{\text{mean}}(\theta, \rho, \sigma) = \frac{\int_{\rho-(v/2)}^{\rho+(v/2)} \check{f}(\theta,\rho,\sigma) d\rho}{v}$ is the mean value of $\check{f}(\theta, \rho, \sigma)$ over v.

While θ is held constant, ρ and σ are varied in the same manner as before to create a new "transform-variance" domain, which is the same size as the original transform domain. The two bright areas represent the edges of the linear wake component. The bright region at the bottom is merely the result of an undesirable black border near the top of our input SAR image.

We now need to isolate the areas in the transform domain that exhibit the strongest responses. The data is thresholded to create a binary transform domain, eliminating the responses of linear features that do not have distinct edges:

$$\check{f}_{\text{bin}}(\theta, \rho, \sigma) = \begin{cases} 1 & \text{if } \check{f}_{\text{var}}(\theta, \rho, \sigma) > T \\ 0 & \text{if } \check{f}_{\text{var}}(\theta, \rho, \sigma) < T. \end{cases} \tag{4}$$

The threshold T is an important parameter, and represents how strong of a response is necessary to indicate the edge of a linear feature. Since the FSLD algorithm will be used on a wide variety of imagery, a value for T must be chosen for the particular imagery being analyzed. In general, a higher level of noise power (variance) in the image will necessitate the use of a higher threshold T to suppress false alarms caused by the background noise. Since it is possible that this thresholding operation will serve to eliminate the responses of some real linear features, a tradeoff must be made between detection rate and false alarm rate. To analyze SAR imagery for ship wakes, a proper choice for T will depend on the characteristics, including incidence angle, of that particular SAR system. This is because the appearance in the SAR image of both ship wakes and naturally-occurring ocean features depends on these characteristics. For our research, the available dataset of SAR imagery was too limited to allow a detailed analysis of the T parameter. However, it was generally true that a wide range of T values would be sufficient to locate the ship wakes but suppress the background noise. For this example, a threshold of $T = 125$ was used. Notice that the undesired response at the bottom is still present.

The next step is the FSLD algorithm is to search the transform space for pairs of responses separated by short intervals in the ρ parameter. Such a pair of responses indicates the two edges of a linear feature in the input image. This search is accomplished through morphological operations on the binary transform space. First, the transform space is dilated by a structuring element that is symmetrical about the origin and extends across the entire transform space in the σ direction, but has a fixed width in the ρ direction. The effect of this operation is that every pixel in the binary transform domain is replaced by a vertical line segment of a certain length. If two responses are close enough in the vertical direction, they will be joined into one.

Then the transform space is eroded by a structuring element that is similar to the previous one, but which has a greater width in the ρ direction. This causes every vertical line in the transform domain of the appropriate length to be replaced by a single pixel. The effect of this operation is that responses that are too narrow in the vertical direction will disappear entirely, while responses which are wide enough will be contracted vertically. By choosing appropriate structuring elements, i.e., dilation and erosion lengths, we can determine the width of the linear features that will be detected.

For this example, the structuring element for dilation was 8 pixels wide, and for erosion it was 16 pixels wide. Notice that the pair of responses representing the wake component have been collapsed into a narrower one that represents the center of the linear feature. The length of the response in the σ direction indicates that the linear feature is longer than the original integration length λ used in the calculation of the localized Radon transform, which was 128 pixels. Notice also that the

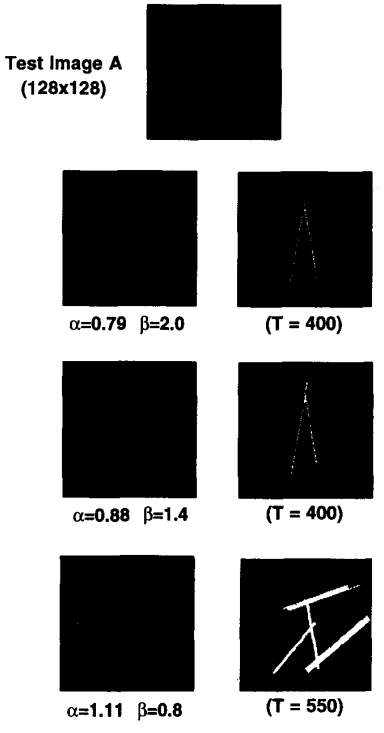

Other Parameters :

$\lambda=\frac{d}{2}$=64 pixels	variance calc. length (υ) = 5 pixels
θ increment = 10°	dilation length = 5 pixels
σ increment (i) = 4 pixels	erosion length = 10 pixels

Fig. 8. Results of the FSLD algorithm on synthetic test image A (simulated bright wake).

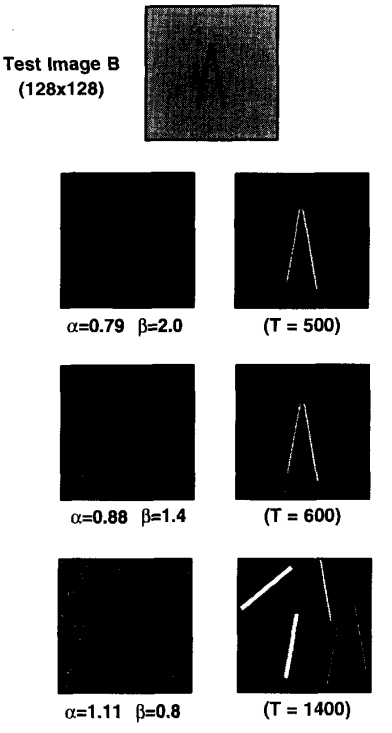

Other Parameters :

$\lambda=\frac{d}{2}$=64 pixels	variance calc. length (υ) = 5 pixels
θ increment = 10°	dilation length = 5 pixels
σ increment (i) = 4 pixels	erosion length = 10 pixels

Fig. 9. Results of the FSLD algorithm on synthetic test image B (simulated dark wake).

undesired response at the bottom has been eliminated. This is because it did not have a neighboring response to join with during dilation, so the process of erosion caused it to disappear completely. Thus, we have accomplished further suppression of false alarms.

The responses that have survived the transform domain processing represent the detected linear features. The only task left for this particular value of θ is to locate the linear features in the image domain that have been detected, if any. This is accomplished by drawing a line of length λ in the image domain for every point remaining in the transform domain. For our example, all of these points lie along a line in the σ direction. This means that the line segments overlap, leaving one line that is longer than λ. The length and location of this line should correspond very closely to the linear feature that was detected.

IV. Experimental Results and Analysis

A. Testing on Synthetic Images

A set of synthetic test images was created to test the FSLD algorithm in a variety of situations. It was desired to test the algorithm's ability to detect both bright and dark linear features, both straight and curved features, and multiple features in the same image. It was also desirable to be able to control the level of noise present in the images. Four of these synthetic images and the results of the FSLD algorithm performed upon them are shown in Figs. 8–11. In each case, the original 128 × 128 synthetic image is shown at the top. Then the same image corrupted by three varying amounts of multiplicative Weibull noise are shown below, with the result of the FSLD algorithm to the right. The value of the threshold T that was used is shown below each result.

The Weibull probability distribution is a generic model for radar noise that has been demonstrated to provide a good approximation under many different imaging conditions [18]. The first-order Weibull probability distribution is:

$$W(y) = \Pr\{n_{xy} \leq y\} = 1 - e^{-\alpha y^{\beta}} \tag{5}$$

where n_{xy} is the noise level at position (x, y) and α and β are scale and shape parameters. If $\beta = 2$, it is the Rayleigh distribution. Three different noise images obeying Weibull statistics were created. Each noise image was characterized by a different pair of scale and shape parameters: $\alpha = 0.79$, $\beta = 2.0$; $\alpha = 0.88$, $\beta = 1.4$; $\alpha = 1.11$, $\beta = 0.8$. Each of these parameter pairs results in a noise function with

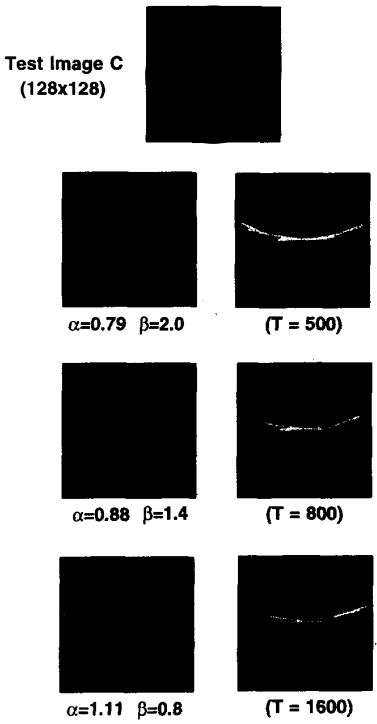

Other Parameters :

$\lambda=\frac{d}{4}$=32 pixels	variance calc. length (υ) = 5 pixels
θ increment = 4°	dilation length = 5 pixels
σ increment (i) = 4 pixels	erosion length = 10 pixels

Fig. 10. Results of the FSLD algorithm on synthetic test image C (curved linear feature).

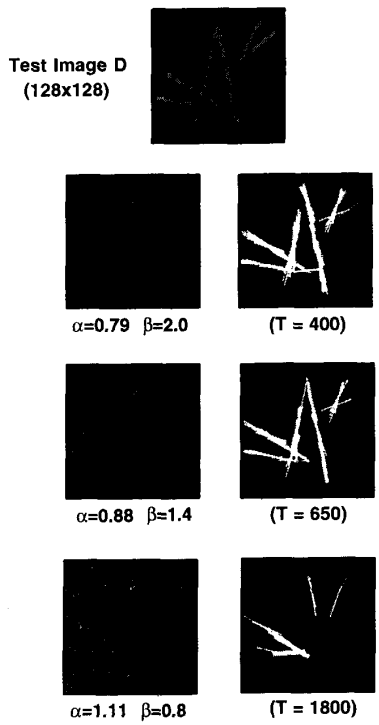

Other Parameters :

$\lambda=\frac{d}{4}$=32 pixels	variance calc. length (υ) = 5 pixels
θ increment = 5°	dilation length = 5 pixels
σ increment (i) = 4 pixels	erosion length = 10 pixels

Fig. 11. Results of the FSLD algorithm on synthetic test image D (multiple simulated wakes).

unity means. Each pixel in these noise functions was created randomly according to the appropriate probability distribution, independent of every other pixel. Then each of the noise functions was multiplied, pixel by pixel, by each of the four synthetic test images. In each of the uncorrupted test images, the pixel intensity of the bright areas was uniformly set to 160, and the pixel intensity of the dark areas was uniformly set to 96. Lower values of the Weibull shape parameter β result in higher levels of noise variance, and thus a lower resulting signal-to-noise ratio.

Fig. 8 shows the results as applied to a simulated V-shaped ship wake (test image A). The straight-line arms of the V-shape meet at an angle of 20°. The FSLD algorithm performed very well for the first two noise-corrupted images, but as the level of multiplicative noise is increased even further ($\beta = 0.8$), the noise variance causes several false alarms in the results. This is not surprising, considering that the synthetic V-shape is virtually indistinguishable in this high level of noise. In test image B (Fig. 9), the V-shape is darker than the background. Again, the algorithm performed very well except for the case where $\beta = 0.8$.

In Fig. 10, the synthetic image is a single curved linear feature. This test image demonstrates how a short integration length λ can better detect linear features that display some curvature. This test image was corrupted by the same multiplicative noise as before, and applied to the FSLD algorithm. With a sufficiently short integration length ($\lambda = \frac{d}{4} = 32$ pixels) for the localized Radon transform, the FSLD algorithm has no difficulty finding the piecewise linear segments of the curve, even in the highest level of noise. In Fig. 11, the synthetic image contains multiple V-shapes of variable sizes. The integration length here was once again $\lambda = \frac{d}{4} = 32$ pixels. Once again, the algorithm has little trouble in the lower levels of noise, but with $\beta = 0.8$, if the threshold was lowered below $T = 1800$ the results were swamped with false alarms.

B. Testing on Real Images

The FSLD algorithm was also tested on three 256 × 256 SAR images of ship wakes. Fig. 12 shows the results for SAR image A, which is the same image that was used earlier in demonstrating the algorithm. The detected linear features using three different threshold levels are shown superimposed on the input image. Notice how lowering the threshold allowed less distinct linear features to be detected. The best result occurred with $T = 125$, when both arms of the V-shaped "Kelvin" wake were detected as well as the bright turbulent wake which extends directly behind the ship. The other parameters were chosen to optimally detect lines about 8 pixels wide. Fig. 13

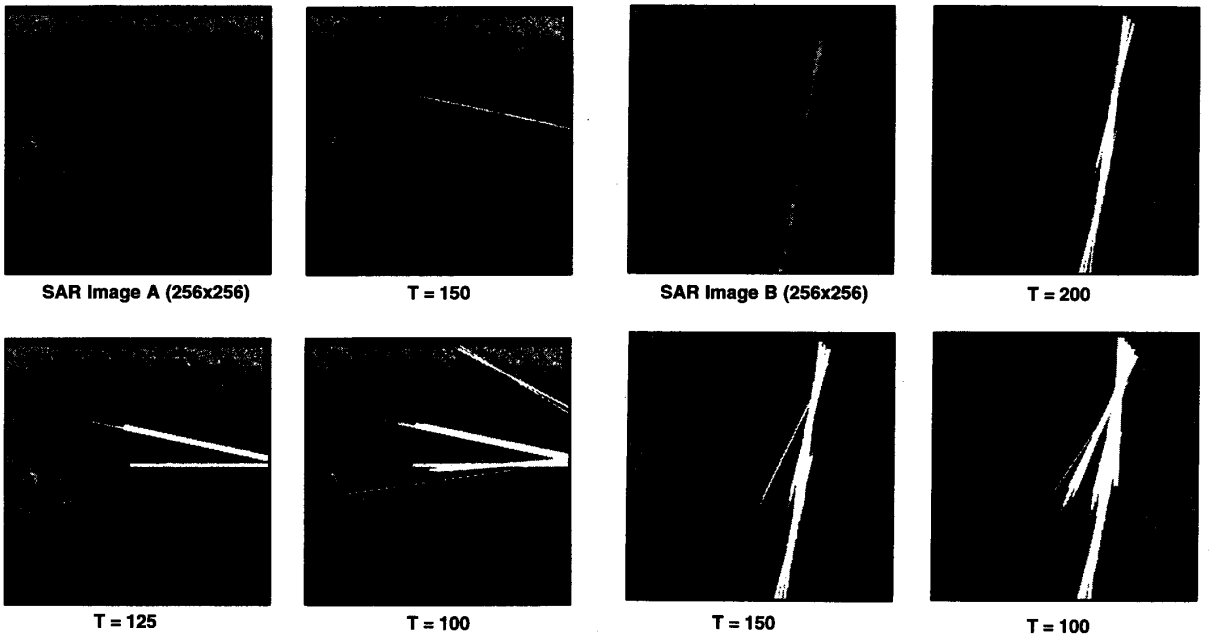

Fig. 12. Results of the FSLD algorithm on SAR image A.

Fig. 13. Results of the FSLD algorithm on SAR image B.

shows the results for SAR image B. The wake components in this image were relatively distinct, so they were picked up nicely by the algorithm. Fig. 14 shows the results for SAR image C. The broad, dark wake component was the most easily detected. The other wake component was detected as the threshold was lowered, but false alarms began to appear quickly. These false alarms were caused by the extremely bright region which is the SAR return of the ship itself. Notice how this bright region appears to be shifted downward from the vertex of the V-shaped wake. Integrating through this bright region produces a much higher value than integrating along a line segment that lies just off of this region. This produces edges in the transform domain that resemble the edges produced by true linear features. Such bright regions caused by actual ship returns would most likely be identified and suppressed prior to application of the algorithm.

Fig. 15 is another example of the FSLD algorithm, applied to two different 160 × 160 images of vehicle tracks in a desert environment. These images have no appreciable noise, but are good examples of the performance of the algorithm for remote surveillance applications using imagery other than SAR. The integration length λ was $\frac{d}{s} = 20$ pixels in both examples, and this was adequate for detecting the curved tracks in the top image and the thin, faint tracks in the lower image. Linear and curvilinear features in a desert scene can be a good indication of vehicle traffic.

V. Conclusions and Future Research Directions

One contributions of this work is a localization of the Radon transform where the intensity integration is performed over a line segment of a particular length rather than across the entire image. This localization results in more distinct peaks in the transform domain for linear features that are much shorter than the image dimensions. It also achieves better spatial localization, enabling us to locate the endpoints of these shorter features. Many existing Radon-based algorithms for linear feature detection could make use of this localization, to potentially achieve higher detection rates and endpoint identification of short line segments.

Another contribution of this work is the FSLD algorithm for linear feature detection in the presence of noise which utilizes this localized Radon transform. This algorithm defines a linear feature not only in terms of its longitudinal characteristics but also its transverse characteristics. The detection of a linear feature's edges occurs within the feature space, or transform domain. The algorithm can be applied to any type of imagery by choosing the appropriate input parameters of the background noise conditions and the target feature dimensions. The algorithm was applied to both synthetic images and actual SAR images of ship wakes. The results of this testing reveal the robustness of the algorithm in high levels of noise and the improved localization of short linear features achieved by reducing the integration length used in

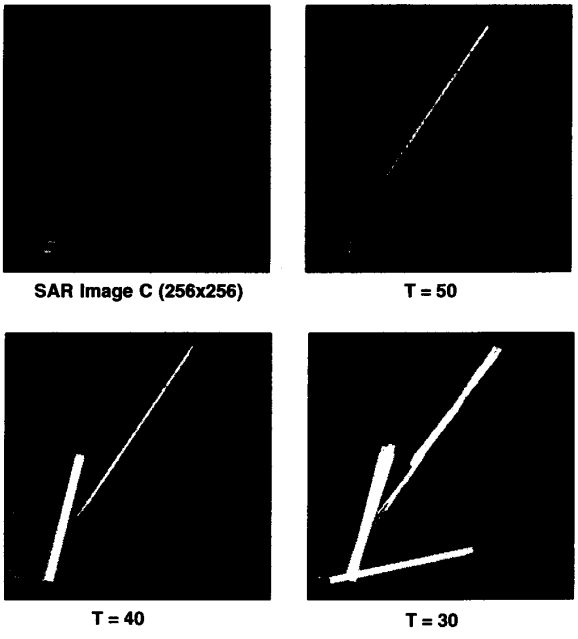

Fig. 14. Results of the FSLD algorithm on SAR image C.

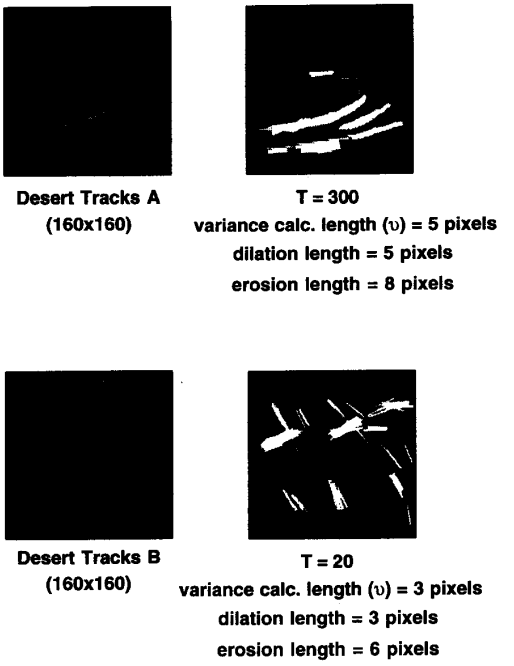

Fig. 15. Results of the FSLD algorithm on two images of vehicle tracks in a desert.

the Radon transform. It is evident that this algorithm, when applied to SAR imagery, should be most appropriate for steep radar depressions, where shadowing will not obscure wake feature edges.

The FSLD algorithm only identifies the linear features in the SAR image. Further work is necessary to develop a complete system for automated surveillance of shipping utilizing SAR imagery. After the linear features in an image have been detected, it is essential to classify these features as to whether they are the result of naturally occurring ocean phenomena or of a ship in motion. A set of linear features extending radially from one point is a good indication that these features comprise a ship wake pattern. It is also known that in sufficiently deep water, all wake structure other than internal waves is contained within a limiting angle of approximately 39°, called the Kelvin angle [19]. This means that any linear features that intersect at an angle greater than 39° do not constitute the Kelvin wake of a moving ship. Once this classification process is complete, it is necessary to analyze the linear wake components to approximate the position and heading of the ship(s) that caused them. To accomplish this, at least two linear wake features must have been identified as created by the same ship. If the system can also identify the SAR signature of the ship itself, its displacement from the estimated actual ship position can yield a calculation for the approximate ship speed. Such a system should probably include some automated process to catalogue and/or analyze this surveillance information.

REFERENCES

[1] M. T. Rey, J. K. E. Tunaley, J. T. Folinsbee, P. A. Jahans, J. A. Dixon, and M. R. Vant, "Application of Radon transform techniques to wake detection in Seasat-A SAR images," *IEEE Trans. Geosci. Remote Sensing*, vol. 28, pp. 553–560, July 1990.

[2] R. F. Gasparovic, D. R. Thompson, and J. R. Apel, "Synthetic aperture radar imaging of ship-generated internal waves," *John Hopkins APL Tech. Dig.*, vol. 10, no. 4, pp. 326–331, 1989.

[3] L. M. Murphy, "Linear feature detection and enhancement in noisy images via the Radon transform," *Pattern Recognition Lett.*, vol. 4, no. 4, pp. 279–284, Sept. 1986.

[4] I. J. Cox, R. A. Boie, and D. A. Wallach, "Line recognition," in *Proc. IEEE 10th Int. Conf. Pattern Recognition*, Atlantic City, NJ, June 1990.

[5] D. H. Ballard and C. M. Brown, *Computer Vision*. Englewood Cliffs, NJ: Prentice Hall, 1982.

[6] C. A. Lipari, M. M. Trivedi, and C. A. Harlow, "Geometric modeling and recognition of elongated regions in aerial images," *IEEE Trans. Syst. Man Cybernet.*, vol. 19, pp. 1600–1612, Nov./Dec. 1989.

[7] A. C. Copeland, G. Ravichandran, and M. M. Trivedi, "Localized Radon transform-based detection of linear features in noisy images," in *Proc. 1994 Conf. Computer Vision and Pattern Recognition*, Seattle, WA, June 1994.

[8] J. Skingley and A. J. Rye, "The Hough transform applied to SAR images for thin line detection," *Pattern Recognition Lett.*, vol. 6, no. 1, pp. 61–67, June 1987.

[9] K. Eldhuset, "Automated ship and ship wake detection in spaceborne SAR images from coastal regions," in *Proc. IGARSS*, Edinburgh, Scotland, Sept. 1988.

[10] ——, "Principles and performance of an automated ship detection system for SAR images," in *Proc. IGARSS*, 1989.

[11] G. G. Hogan, J. B. Marsden, and J. C. Henry, "On the detection of internal waves in high resolution imagery using the Hough transform," in *Proc. from Oceans*, 1991.

[12] M. T. Rey, T. Sibbald, and J. K. E. Tunaley, "Application of the Dempster–Shafer algorithm to the detection of SAR ship wakes," in *Proc. IGARSS*, 1992.

[13] C. D. Knittle and N. Magotra, "Enhancement and detection of ship wakes in synthetic aperature radar images," Rep. SAND91-2118, Sandia National Laboratories, Oct. 1991.
[14] J. Radon, "Über die Bestimmung von Funktionen durch ihre Integralwerte längs gewisser Mannigfaltigkeiten, *Berichte Sächsische Akademie der Wissenschaften. Leipzig, Math.–Phys. Kl.*, vol. 69, pp. 262–267, 1917.
[15] P. V. C. Hough, "Method and means for recognizing complex patterns," U. S. Patent 3 069 654, 1962.
[16] S. R. Deans, "Hough transform from the Radon transform," *IEEE Trans. Pattern Anal. Mach. Intell.*, vol. PAMI-3, pp. 185–188, Mar. 1981.
[17] A. Califano and R. Bolle, "The multiple window parameter transform," *IEEE Trans. Pattern Anal. Mach. Intell.*, vol. 14, pp. 1157–1170, Dec. 1992.
[18] R. Brooks and A. Bovik, "Robust techniques for edge detection in multiplicative Weibull image noise," *Pattern Recognition*, vol. 23, no. 10, pp. 1047–1057, 1990.
[19] J. F. Vesecky and R. H. Stewart, "The observation of ocean surface phenomena using imagery from the SEASAT synthetic aperture radar: An assessment," *J. Geophys. Res.*, vol. 87, no. C5, pp. 3397–3430, Apr. 1982.

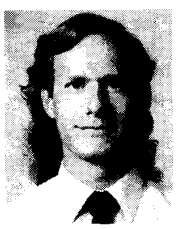

Anthony C. Copeland received the B.S.E.E. degree from the U.S. Military Academy, West Point, NY, in 1988, and the M.S.E.E. degree from the University of Tennessee, Knoxville, in 1993. He is currently pursuing the Ph.D. degree at the same institution.

He served as a signal corp (communications) officer in the U. S. Army from 1988 to 1991. During his military service, he served as a communications node platoon leader from the 24th Infantry Division (Mechanized) based in Fort Stewart, GA. This service included participation in both Operation Desert Shield and Operation Desert Storm during the Persian Gulf conflict in 1990–1991. He is currently a member of the Computer Vision and Robotics Research Laboratory at the University of Tennessee, Knoxville. His current research interests include computer vision, image understanding, and human visual perception.

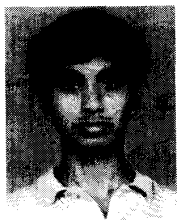

Gopalan Ravichandran received the B.Tech. degree from the Indian Institute of Technology, Madras, in 1987 and the M.S. and Ph.D. degrees from Carnegie Mellon University, Pittsburgh, PA, in 1989 and 1992, respectively.

He is a Research Associate at the Computer Vision and Robotics Research Laboratory at the University of Tennessee, Knoxville. His research interests include the use of digital and optical processing techniques for computer vision and image understanding.

Mohan M. Trivedi received the B.E. degree in electronics from the Birla Institute of Technology and Science, Pilani, India, in 1974 and the M.E. and Ph.D. degrees in electrical engineering from Utah State University, Logan, in 1976 and 1979, respectively.

He is a Professor in the Electrical and Computer Engineering Department of the University of Tennessee, Knoxville. He and his team in the Computer Vision and Robotics Research Laboratory are actively engaged in research in sensor-based mobile manipulators, active perception and machine vision, interactive graphical interfaces for human–machine systems, and remote sensing. He is a frequent consultant to various industrial and government agencies. He regularly offers tutorials (both "in-class" and satellite TV-based) dealing with his specialty areas for professional groups in the U.S. and abroad. He has published over 170 archival papers and has edited over a dozen volumes, including books, special issues, video presentations, and conference proceedings.

Dr. Trivedi is an Associate Editor of the IEEE TRANSACTIONS ON SYSTEMS, MAN, AND CYBERNETICS, *Pattern Recognition*, and the *International Journal of Applied Intelligence*, and is on the editorial boards of the *Machine Vision and Applications Journal*, and the *Optical Engineering Reports*. He served as the chairman of the Robotics Technical Committee of the Computer Society of the IEEE (1987–1989). He chairs the Pattern Recognition, Image Processing and Computer Vision Committee of the IEEE Systems, Man, and Cybernetics Society.

Dr. Trivedi has received the Pioneer Award and the Meritorious Service Award of the IEEE Computer Society. In 1993, he received the Distinguished Alumnus Award form Utah State University. He is a Fellow of SPIE. He has been elected to the honor societies of Phi Kappa Phi, Tau Beta Pi, and Sigma Xi.